Estimating the total ultrasound attenuation along the propagation path by using a reference phantom

Yassin Labyed and Timothy A. Bigelow[a)]
Department of Electrical and Computer Engineering, Iowa State University, 2113 Coover Hall, Ames, Iowa 50011

(Received 28 April 2010; revised 5 August 2010; accepted 6 August 2010)

In this study, an algorithm previously developed for estimating the total ultrasonic attenuation along the propagation path from the surface of the transducer to a region of interest (ROI) in tissue, was modified to make it more practical for use in clinical settings. Specifically, the algorithm was re-derived for when a tissue mimicking phantom rather than a planar reflector is used to obtain the reference power spectrum. The reference power spectrum is needed to compensate for the transfer function of the transmitted pulse, the transfer function of transducer, and the diffraction effects that result from focusing/beam forming. The modified algorithm was tested on simulated radio frequency (RF) echo lines obtained from two samples that have different scatterer sizes and different attenuation coefficient slopes, one of which was used as a reference. The mean and standard deviation of the percent errors in the attenuation coefficient estimates (ACEs) were less than 5% and 10%, respectively, for ROIs that contain more than 10 pulse lengths and more than 25 independent echo lines. The proposed algorithm was also tested on two tissue mimicking phantoms that have attenuation coefficient slopes of 0.7 dB/cm-MHz and 0.5 dB/cm-MHz respectively, the latter being the reference phantom. When a single element spherically focused source was used, the mean and standard deviation of the percent errors in the ACEs were less than 5% and 10% respectively for windows that contain more than 10 pulse lengths and more than 17 independent echo lines. When a clinical array transducer was used, the mean and standard deviation of the percent errors in the ACEs were less than 5% and 25%, respectively, for windows that contain more than 12 pulse lengths and more than 45 independent echo lines.
 [DOI: 10.1121/1.3483739]

PACS number(s): 43.80.Qf, 43.20.Hq, 43.20.Fn, 43.80.Cs [CCC] Pages: 3232–3238

I. INTRODUCTION

Knowing the total ultrasonic attenuation along the propagation path from the transducer surface to the ROI in the sample is essential in many medical ultrasound applications. In the area of ultrasonic tissue characterization, accurate estimates of the scatterer size and the backscatter coefficient can only be obtained if the total attenuation is known (Kuc, 1980; Oelze *et al.*, 2004; Bigelow *et al.*, 2008). In ultrasound therapy applications, the total attenuation is used to calculate the intensity of ultrasound that reaches the region of interest (ROI) and hence quantify the amount of heating that is produced (Parmar and Kolios, 2004, 2006). In ultrasonic imaging, time gain compensation can be done more accurately if the total attenuation is known, and therefore eliminate shadowing and enhancement regions in the image (Treece *et al.*, 2005). In acoustic radiation force imaging, the total attenuation is used to quantify the amount of radiation force applied to the ROI (Starritt *et al.*, 1991; Callé *et al.*, 2005). Therefore many areas of clinical medical ultrasound would benefit from an accurate estimate of the total attenuation along the propagation path.

Traditionally, the total attenuation was estimated by measuring changes in the backscatter intensity with depth (He, 1986; Tu *et al.*, 2006). However, this method is inaccurate because the attenuation, the backscatter, and the diffraction effects modify the power spectrum of the backscattered RF signals. Some investigators estimated the local attenuation and thickness of the overlying tissues along the propagation path and then performed a weighted sum of these estimates to calculate the total attenuation (Lizzi *et al.*, 1983; Sidney, 1997). These methods, however, are prone to error accumulation with propagation depth. Furthermore, they require the identification of the different overlying tissues, a process that may require manual intervention. Another approach, termed the Spectral Fit Algorithm, attempted to simultaneously estimate the total attenuation and the scatterer properties from the backscattered RF signals (Bigelow and O'Brien, 2004; Bigelow *et al.*, 2005). However, these estimates had poor precision and required knowing the scattering model in advance. Recently, we developed a new algorithm that estimates the total attenuation by processing echoes from multiple ultrasound sources that are used to scan the same tissue region (Bigelow, 2008). To remove the requirement of multiple sources, this algorithm was later modified by applying Gaussian filters to the power spectrum of the backscattered RF data from the ROI (Bigelow, 2010b). Unlike other techniques, this algorithm is independent of the intervening tissue layers leading to the ROI and requires no prior knowledge of the scatterer size, the scatterer density and the scattering strength.

[a)]Author to whom correspondence should be addressed. Electronic mail: bigelow@iastate.edu

In this study, we modified the algorithm that we used in our earlier work for total attenuation estimation (Bigelow, 2008, 2010b) by employing a tissue mimicking reference phantom (TMP) instead of a planar reflector to compensate for the transfer function of transducer and the diffraction effects that result from focusing. The TMP has a known attenuation coefficient and a propagation sound speed that closely matches the sound speed in soft tissue. The method of using a reference phantom to compensate for the electromechanical properties of the transducer and the diffraction effects has been demonstrated before, and was used in measuring the backscatter coefficient and the local ultrasonic attenuation within a ROI in soft tissue using clinical array sources (Insana *et al.*, 1983; Yao *et al.*, 1990). Using a tissue mimicking reference phantom makes the algorithm practical for use in clinical settings where beam formed echoes are obtained from array sources. The objective of this paper is to re-derive our earlier algorithm (Bigelow, 2010b) for when a TMP is used as a reference, and to test its accuracy using computer simulations and on TMPs with known attenuations and scattering properties. Both a spherically focused transducer and a clinical array transducer were used to obtain RF backscattered signals from the two TMPs. One of the TMPs was used as a reference to estimate the attenuation coefficient in the other phantom.

II. DERIVATION OF ALGORITHM

In order to estimate the total ultrasonic attenuation from the surface of the transducer to an ROI in a sample, the same transducer and power settings are used to obtain backscattered signals from the sample, and from a tissue mimicking reference phantom. The TMP has a known attenuation coefficient and a propagation sound speed that closely matches the sound speed in soft tissue. Each RF echo line is windowed at the ROI to form multiple adjacent time gated windows. The Fourier Transform is applied to every window, and the power spectra of the windows are averaged. The same procedure is performed on the region of the reference phantom that has the same compared depth as the ROI of the sample. In standard pulse echo imaging, the measured power spectrum of a windowed region in a statistically homogeneous tissue is given by

$$S_s(f,d) \propto A_s(f) \times D_s(d,f) \times F_s(f) \times H(f) \times F_{att}(d,f,\alpha_1,\alpha_2,\ldots,\alpha_N). \quad (1)$$

This equation assumes that the windows used to gate the echoes are small compared to the depth of focus for the transducer so that the variations of the field within each gated region could be ignored (Bigelow and O'Brien, 2006). The subscript s denotes the sample. d is the distance from the surface of the transducer to depth that corresponds to the center of the time gated window. $A_s(f)$ is the power spectrum of the transmitted pulse. $D_s(d,f)$ is a diffraction term that results from focusing. $F_s(f)$ is a frequency dependent term that results from the scattering properties of the ROI. $H(f)$ is the transfer function of the ultrasound source. Lastly, F_{att} is the total frequency-dependent attenuation along the path and can be written as

$$\begin{aligned} F_{att}(d,f,\alpha_1,\alpha_2,\ldots,\alpha_i,\ldots\alpha_N) &= \exp(-4\alpha_1 d_1 f^{n_1}) \times \exp[-4\alpha_2(d_2-d_1)f^{n_2}] \times \ldots \\ &\times \exp[-4\alpha_i(d_i-d_{i-1})f^{n_i}] \times \ldots \\ &\times \exp[-4\alpha_{N-1}(d_N-d_{N-1})f^{n_{N-1}}]. \end{aligned} \quad (2)$$

d_i is the distance from the surface of the transducer to the end of the ith intervening tissue layer. $(\alpha_1,\alpha_2,\ldots,\alpha_N)$ are the attenuation coefficient slopes of the intervening tissues leading to the ROI; each having a frequency dependence of n_i. The total frequency dependent attenuation along the propagation path can be assumed linearly dependent on frequency. This is a reasonable assumption over the frequency range of most transducers (Wear, 2002). Hence, the attenuation coefficient can be written as

$$\alpha = \alpha_s f, \quad (3)$$

where α_s is the total attenuation coefficient slope. The total frequency-dependent attenuation along the path can be written as

$$F_{att}(d,f,\alpha_1,\alpha_2,\ldots,\alpha_i,\ldots\alpha_N) \simeq \exp(-4\alpha_s df). \quad (4)$$

Similarly, the power spectrum of the backscattered signal from the reference phantom is

$$S_r(f,d) \propto A_r(f) \times D(d,f) \times F_r(f) \times H(f) \times \exp(-4\alpha_r df). \quad (5)$$

The subscript r denotes the reference phantom. The transfer function of the transmitted pulse in the sample is equal to the transfer function of the transmitted pulse in the reference phantom if the reflection coefficient of the front surface of the sample is the same as the reflection coefficient of the front surface of the phantom. However, if the reflection coefficients are different, we have

$$A_s(f) = cA_r(f), \quad (6)$$

where c is constant. The diffraction terms $D_s(d,f)$ and $D_r(d,f)$ in Eqs. (1) and (5) are equal if we assume that the sound speed is the same in the sample and the reference. Dividing the power spectrum of the sample by the power spectrum of the reference phantom yields

$$\frac{S_s}{S_r} \propto \frac{F_s(f)}{F_r(f)} \times \exp(-4df\Delta\alpha), \quad (7)$$

where

$$\Delta\alpha = (\alpha_s - \alpha_r). \quad (8)$$

Insana and Hall (1990)and Insana *et al.* (1990) showed that the scattering terms can be written as

$$F_s(f) \propto f^4 \times F_{\gamma s}(f,a_{eff\_s}), \quad (9)$$

$$F_r(f) \propto f^4 \times F_{\gamma r}(f,a_{eff\_r}). \quad (10)$$

$F_{\gamma s}(f,a_{eff\_s})$ and $F_{\gamma r}(f,a_{eff\_r})$ are the form factors of the sample and the reference, respectively. a_{eff_s} and a_{eff_r} are the effective scatterer sizes of the sample and the reference, respectively. The form factor is approximated by (Insana *et al.*, 1990)

$$F_\gamma(f,a_{eff}) \propto \exp(-Bf^n), \tag{11}$$

where B is proportional to the correlation length and n is a parameter that varies with the scattering model. The values of n are in the range of 2 for the scattering models used for TMPs and tissue. Equation (7) becomes

$$S(f) = \frac{S_s}{S_r} \propto \frac{\exp(-B_s f^{n_s})}{\exp(-B_r f^{n_r})}\exp(-4df\Delta\alpha),$$

$$S(f) \propto \exp(-\Delta B f^n)\exp(-4df\Delta\alpha), \tag{12}$$

where $\Delta B = B_s - B_r$ and $n_s \cong n_r \cong n$.

If we multiply (12) by a Gaussian Filter with a center frequency f_c and a variance σ_c^2, we obtain

$$S(f) \propto \exp(-\Delta B f^n)\exp(-4df\Delta\alpha)\exp\left[-\frac{(f-f_c)^2}{2\sigma_c^2}\right]. \tag{13}$$

We can then approximate $\Delta B f^n$ using Taylor series to get

$$\Delta B f^n \cong \Delta B\left[f_c^n + n(f-f_c)f_c^{n-1} + \frac{n(n-1)(f-f_c)^2 f_c^{n-2}}{2}\right], \tag{14}$$

yielding

$$S(f) \propto \exp\left[-\frac{(f-\tilde{f}_c)^2}{2\tilde{\sigma}_c^2}\right], \tag{15}$$

where

$$\tilde{\sigma}_c^2 = \frac{\sigma_c^2}{1-\sigma_c^2\Delta B n f_c^{n-2}},$$

$$\tilde{f}_c = [1-\tilde{\sigma}_c^2\Delta B n(n-1)]f_c + (4d\tilde{\sigma}_c^2)\Delta\alpha. \tag{16}$$

Equation (15) shows that the resulting spectrum is also Gaussian with a new center frequency $\tilde{f}_c$ which is a function of the scattering properties, attenuation, and the center frequency of the Gaussian filter. Based on Eq. (16), $\Delta\alpha$ can be estimated by finding the intercept of the line that fits the new center frequencies, $\tilde{f}_c$, with respect to the center frequencies of the Gaussian filters. Once $\Delta\alpha$ is known, the slope of the total attenuation coefficient in the unknown sample can be determined.

III. SIMULATIONS PROCEDURE AND RESULTS

Computer simulations were used to obtain two different data sets of RF backscattered signals using a Gaussian focused beam (5 cm focal length, 0.62 mm beamwidth, 7.5 MHz center frequency, and 50% −3 dB bandwidth on transmit). One data set is used as a sample while the other is used as reference. The sample and reference had attenuation coefficients of 0.7 dB/cm-MHz and 0.5 dB/cm-MHz, respectively. The sample scatterers had a Gaussian Form Factor with 20 μm effective radii. The reference had spherical shell scatterers with 10 μm radii. The spatial pulse length is 0.385 mm. Both the sample and the reference had a scattering density of 100 mm^{-3}, corresponding to approximately 10 scatterers per resolution cell, which is adequate for fully developed speckle (Bigelow and O'Brien, 2004).

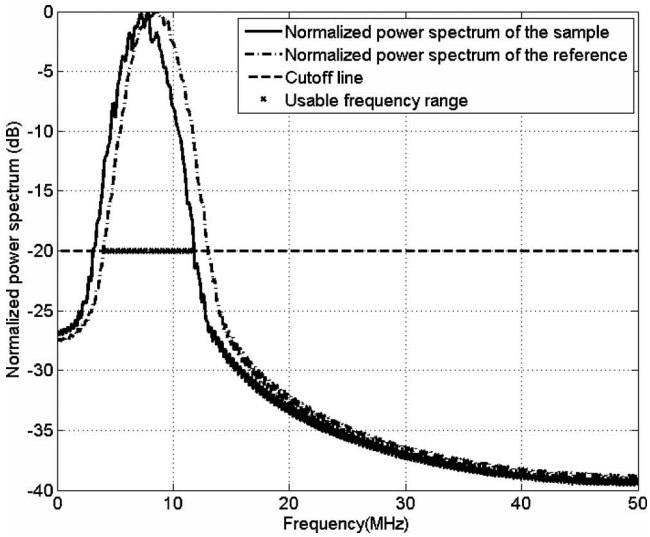

FIG. 1. A plot of the normalized power spectrum obtained from averaging 50 power spectra from the sample and the reference in the simulations.

In the simulations, 3000 independent echo lines were generated for the sample and 300 independent echo lines were generated for the reference. Each RF echo line was gated with a rectangular window centered at the focus. The power spectrum of each time gated window is approximated by taking the Fourier Transform of the RF data and squaring the magnitude of the result. In order to operate above the noise floor, the usable frequency range was selected to be the frequencies common to the −20 dB bandwidths of the sample and reference spectrum as is illustrated in Fig. 1.

After determining the usable frequency range, the usable power spectrum of the sample was divided by the usable power spectrum of the reference. The resulting spectrum S, was then multiplied by three Gaussian filters that have center frequencies within the usable frequency range, and that form 4 equally spaced intervals within this range. For easy comparison, the spectra were multiplied by the three Gaussian filters as was done in the previous studies by Bigelow (Bigelow, 2008, 2010a). In a future paper, we will find the optimal number of Gaussian filters. The three Gaussian filters have the same 3-dB percent bandwidth. The 3-dB percent bandwidth is chosen such that the minimum frequency in the usable frequency range corresponds to −15 dB of the power spectrum that results from multiplying S by the Gaussian filter that has the smallest center frequency. The ratio of the power spectrum of the sample to the power spectrum of the reference is multiplied by a fourth Gaussian filter (as was done in the previous studies by Bigelow) that has a center frequency that corresponds to the middle of the usable frequency range, and variance that corresponds to the variance of a Gaussian function that fits the power spectrum of the sample. After multiplying the four Gaussian filters by the ratio of the power spectrum of the sample to power spectrum of the reference, we obtained four different spectra which are also Gaussian. The spectra are fit to a Gaussian function in

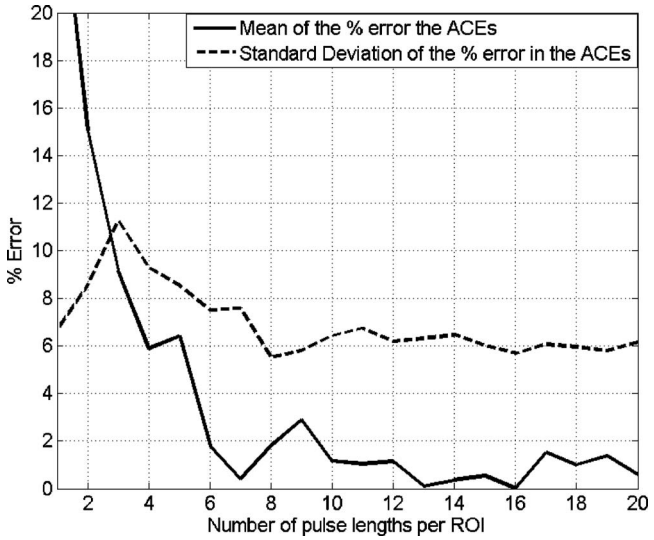

FIG. 2. Plot of the absolute value of the mean and the standard deviation of the percent error in the attenuation coefficient estimates that were obtained using a Gaussian focused beam in the simulations, for regions of interest that contain 50 independent echo lines, versus the number of pulse lengths per region of interest.

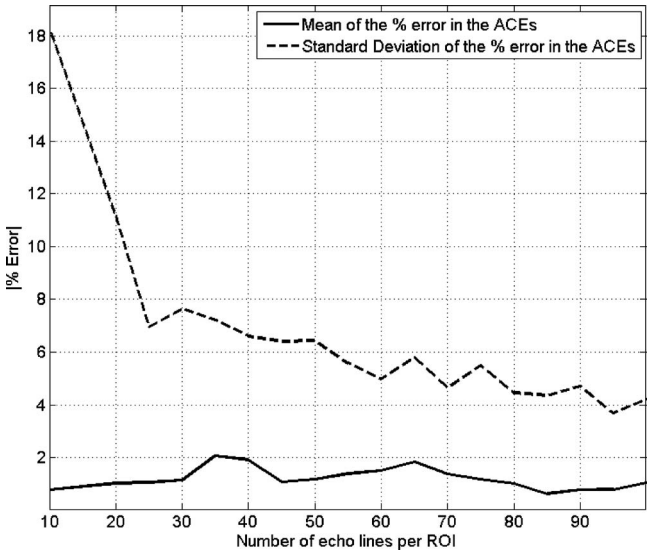

FIG. 3. Plot of the absolute value of the mean and the standard deviation of the percent error in the attenuation coefficient estimates that were obtained using a Gaussian focused beam in the simulations, for regions of interest that are 10 pulse lengths long, versus the number of independent echo lines per region of interest.

order to find the center frequencies $\tilde{f}_c$ and the variances $\tilde{\sigma}_c^2$. According to Eq. (16), the attenuation coefficient slope is estimated by finding the intercept of the line that fits the center frequencies of the new Gaussian spectra versus the center frequencies of the Gaussian filters. This intercept is then divided by $4d\tilde{\sigma}_c^2$.

To find how the error in the ACEs changes with respect to the ROI size, we fixed the number of independent echo lines per estimate to 50 and varied the size of the ROI from 1 pulse length to 20 pulses lengths, and we obtained 30 estimates for each combination. We measured the pulse length as the duration from the first transition above the 0.1% of the maximum amplitude level to last transition below the 0.1% maximum level. We varied the length of the ROI size in terms of the number of pulse lengths per ROI instead of the number of wavelengths per ROI because it was shown than the optimal ROI size depends on the number of pulse lengths per ROI and not the center frequency of the transducer (Bigelow, 2010b). Figure 2 shows a plot of the absolute value of the mean and the standard deviation of the percent error in the ACEs versus the number pulses per ROI. We observed that the absolute value of the mean and the standard deviation of the percent error in the ACEs are less than 5% and 10%, respectively, for ROIs that contain 6 pulse lengths. The windowing effects are less significant for large time gated windows, and this explains why the mean of the ACEs stabilizes for axial ROIs that are greater than 6 pulse lengths. The STD in the ACEs doesn't change significantly with increasing axial ROI size.

To find how the error in the ACEs varies with the number of independent echo lines per ROI, we set the size of the time gated window (ROI) to 10 pulse lengths and varied the number of averaged power spectra per window for the sample and the reference from 5 to 100 averaged power spectra, and obtained 30 estimates for each combination. Figure 3 shows a plot of the absolute value of the mean and the standard deviation of the percent error in the ACEs versus the number of independent echo lines. We observed that the absolute value of the mean and the standard deviation of the percent error in the ACEs are less than 5% and 10% respectively, for ROIs that contain 25 independent echo lines or more.

IV. TISSUE MIMICKING PHANTOM PROCEDURE AND RESULTS

A. Spherically focused transducer

After completing the computer simulations, we tested our algorithm on two TMPs (Gammex 406 LE 0.7, Gammex 406 LE 0.5) that had attenuation coefficient slopes 0.7 dB/cm MHz and 0.5 dB/cm MHz, respectively. The scattering targets in this phantom are glass beads ($\sim$160 beads/mm^3) with a mean diameter of 35 μm. The phantom with the 0.7 dB/cm MHz attenuation coefficient was chosen as the sample and the phantom with the 0.5 dB/cm MHz attenuation coefficient was chosen as the reference. The two phantoms were scanned using a spherically focused transducer (5.14 cm focal length, f/4, and 7.5 MHz center frequency). The transducer was translated horizontally at 1 mm increments and 1 RF echo was obtained at each position. The step size of 1 mm is larger than the beamwidth of the transducer which was measured to be approximately 0.837 mm. A total of 225 echo lines were obtained for the sample and 45 RF echo lines from the reference. Using a hydrophone, we measured the pulse length of the transducer and found it to be approximately equal to 0.274 mm.

To find how the error in the ACEs changes with respect to the window size, we fixed the number of averaged power spectra per estimate to 45 and varied the size of the window from 1 pulse length to 12 pulses and obtained 5 attenuation coefficient estimates for each combination. Figure 4 shows a plot of the absolute value of the mean and the standard de-

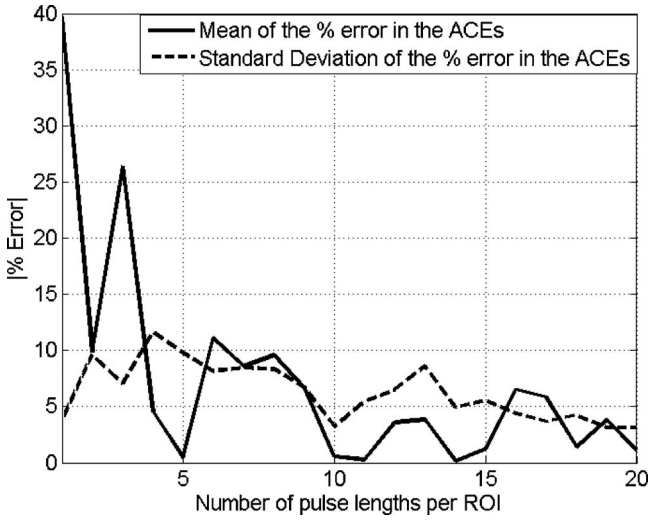

FIG. 4. Plot of the absolute value of the mean and the standard deviation of the percent error in the attenuation coefficient estimates that were obtained using a spherically focused transducer in the phantom experiment, for regions of interest that contain 45 independent echo lines, versus the number of pulse lengths per region of interest.

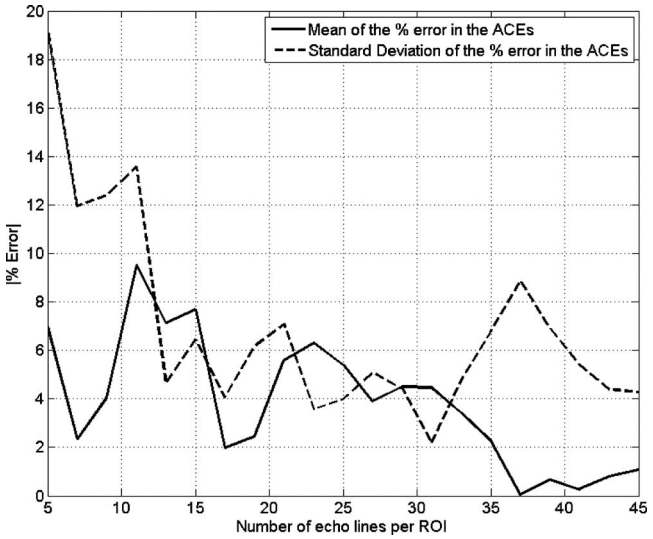

FIG. 5. Plot of the absolute value of the mean and the standard deviation of the percent error in the attenuation coefficient estimates that were obtained using a spherically focused transducer in the phantom experiment, for regions of interest that are 10 pulse lengths long, versus the number of independent echo lines per region of interest.

viation of the percent error in the ACEs versus the number pulses per ROI. We observed that the absolute value of the mean and the standard deviation of the percent error in the ACEs are less than 10% for ROIs that contain 10 pulse lengths or more. A similar behavior was observed in the simulations. Note that there are more fluctuations due to the smaller number of estimates (5 estimates) used to the determine the mean and standard deviation.

To find how the error in the attenuation coefficient estimates varies with the number of independent echo lines per ROI, we fixed the window size to 10 pulse lengths (the optimal number of pulse lengths) and varied the number of averaged power spectra per window for the sample and the reference from 5 to 45 uncorrelated power spectra, and obtained 5 estimates for each combination. Figure 5 shows a plot of the absolute value of the mean and the standard deviation of the percent error in the ACEs versus the number of independent echo lines. We observed that the absolute value of the mean and the standard deviation of the percent error in the ACEs are less than 5% and 10% respectively, for ROIs that contain 17 independent echo lines or more. Figures 4 and 5 have more fluctuations because of the small number of estimates.

B. Clinical array transducer

We used a clinical array transducer (~7 MHz, L8–3 Linear Array Transducer) driven by a clinical ultrasound system (z.one Ultrasound System, ZONARE Medical Systems, Inc.) to obtain 10 RF data sets from the 0.7 dB/cm-MHz phantom and 1 RF data set from the 0.5 dB/cm-MHz phantom. Each set contains 250 RF echo lines. These echo lines are obtained after beamforming, and are used to generate the B-mode image. The ZONARE ultrasound system focuses on receive only and doesn't allow any control of the size pulse length, the number of focal zones, or the location of the focal zones. Using a hydrophone, we measured the pulse length of the transducer to be 0.35 mm. To determine the number of uncorrelated A-lines in the ROI, the correlation coefficient was measured among adjacent A-lines from the reference phantom using the following equation (Hall *et al.*, 1996):

$$\rho = \frac{\sum_{i=1}^{m} [(X_i - \bar{X})(Y_i - \bar{Y})]}{\sqrt{\sum_{i=1}^{m} [(X_i - \bar{X})^2 (Y_i - \bar{Y})^2]}}, \tag{17}$$

where X_i and Y_i are the RF echo amplitudes of A-Lines X and Y, respectively, at position i in the sub region of the echo data. $\bar{X}$ and $\bar{Y}$ are the sample mean values. Figure 6 shows the correlation coefficient between the 100th echo line and the echo lines from 80 to 120. Based on this figure, the correlation coefficient is less than 0.2 between echo lines that

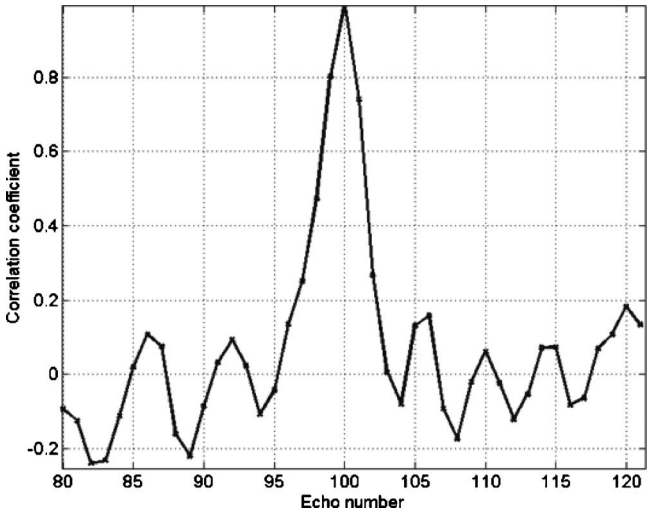

FIG. 6. Plot of the correlation coefficient between the 100th echo line and the echo lines from 80 to 120.

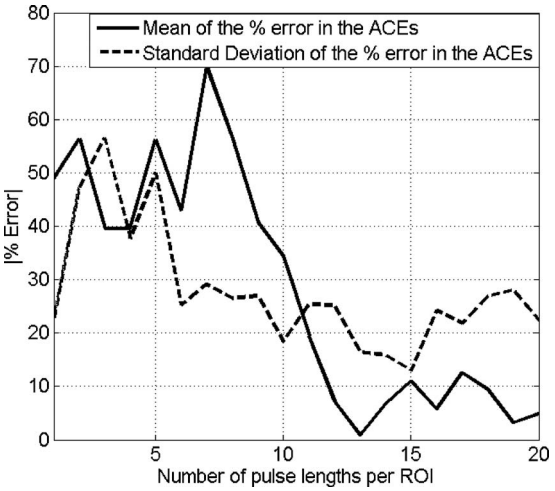

FIG. 7. Plot of the absolute value of the mean and the standard deviation of the percent error in the attenuation coefficient estimates that were obtained using a clinical array transducer in the phantom experiment, for regions of interest that contain 60 independent echo lines, versus the number of pulse lengths per region of interest.

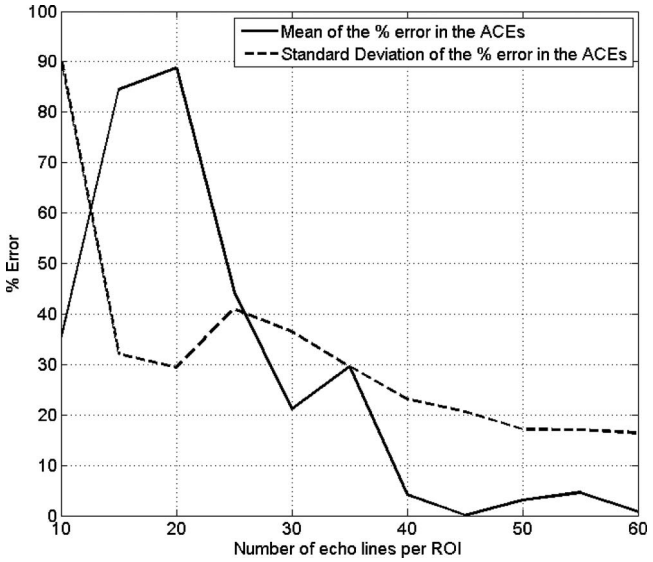

FIG. 8. Plot of the absolute value of the mean and the standard deviation of the percent error in the attenuation coefficient estimates that were obtained using a clinical array transducer in the phantom experiment, for regions of interest that are 12 pulse lengths long, versus the number of independent echo lines per region of interest.

are separated by at least two adjacent lines. Thus with a 20% criterion for de-correlation, we considered the echo lines that are separated by two lines to be uncorrelated.

To find how the error in the ACE changes with respect to the window size, we fixed number of averaged power spectra per estimate to 60 and varied the size of the window from 1 pulse length to 20 pulses and obtained 1 estimate of attenuation in each data set at a depth of 2.25 cm. Figure 7 shows a plot of the absolute value of the mean and the standard deviation of the percent error in the ACEs versus the number pulses per ROI. We observed that the absolute value of the mean and the standard deviation of the percent error in the ACEs are less than 10% and 25% respectively, for ROIs that contain 12 pulse lengths or more.

To find how the error in the attenuation coefficient estimates varies with number of echo lines per ROI, we fixed the window size to 12 pulse lengths (the optimal number of pulse lengths) and varied the number of averaged power spectra per window for the sample and the reference from 10 to 60 averaged power spectra and obtained 10 estimates of attenuation in each combination at a depth of 2.25 cm. Figure 8 shows a plot of the absolute value of the mean and the standard deviation of the percent error in the ACEs versus the number of independent echo lines. We observed that the absolute value of the mean and the standard deviation of the percent error in the ACEs are less than 5% and 20% respectively, for ROIs that contain 45 independent echo lines or more.

V. DISCUSSION AND CONCLUSION

In this paper, we modified an earlier algorithm for estimating the total attenuation along the propagation path by using a TMP instead of a planar reflector to obtain a reference power spectrum and compensate for the transfer function of transmitted pulse, the transfer function of the transducer, and the diffraction effects. This modification allows the new algorithm to be more practical for use in clinical settings. The modified algorithm was verified using computer simulations and phantom experiments. In the simulations, we found that the optimal number of pulse lengths per ROI is 10 and that the optimal number of independent echo lines per ROI is 25. These optimal values result in a mean of percent errors less than 5% and a standard deviation of percent errors less than 10%. When a spherically focused transducer was used on TMPs, we found that the optimal number of pulse lengths per ROI is 10 and that the optimal number of echo lines per ROI is 17. These optimal values result in a mean of percent errors less than 5% and a standard deviation of the percent errors less than 10%. When a clinical array transducer was on the TMPs, we found that the optimal number of pulse lengths per ROI is 12 and that the optimal number of echo lines per ROI is 45. These optimal values result in a mean of percent error less than 5% and a standard deviation of the percent errors less than 20%.

Based on these results, the optimal ROI length in pulse lengths is slightly higher when a clinical array transducer was used, than when a spherically focused transducer was used. This may have resulted due to the difficulty in accurately determining the transmit pulse length of the clinical array transducer. In other words, the pulse length of the clinical array transducer may have been underestimated when it was measured using the hydrophone. The results also showed that the mean and standard deviation of the percent errors in the ACEs are higher when a clinically array transducer was used than when a spherically focused transducer was used. Furthermore, the optimal number of echo lines per ROI was larger when the clinical array transducer was used on the TMPs than the optimal number of echo lines per ROI that was obtained in the simulations, and that the optimal number of echo lines in the simulations was larger than the optimal number of echo lines when the spherically focused transducer was used on the TMPs. To explore this further, we

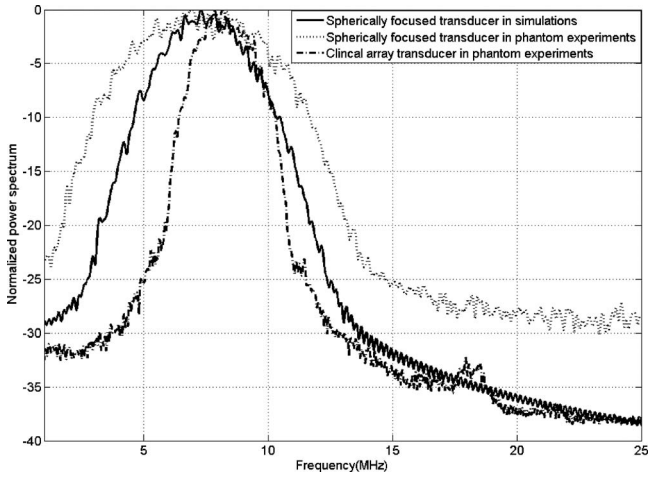

FIG. 9. Plot of the normalized power spectrum versus frequency, for the Gaussian focused beam in the simulations, the spherically focused transducer, and the clinical array transducer.

plotted the normalized power spectra that were obtained using the Gaussian focused beam in the simulations, the spherically focused transducer, and the clinical array transducer in the phantom experiments as shown in Fig. 9. We observed that bandwidth of the clinical array transducer is smaller than the bandwidth of the Gaussian focused beam in the simulations, and that the bandwidth in the simulations is smaller than the bandwidth of the spherically focused transducer. A small bandwidth implies that the usable frequency range is small, and therefore the spacing between the center frequencies of the applied Gaussian filters is also small. When the center frequencies of the Gaussian filters are too close, the fit of the line equation given by Eq. (16) is less accurate because there is not a significant difference between the Gaussian center frequencies $\tilde{f}_c$.

The effects of varying the number of Gaussian filters, the bandwidths of the filters, and the center frequencies are now being studied. The errors that may result from differences in the sound propagation speed between the phantom and the overlying tissues of the sample are also being considered.

ACKNOWLEDGMENTS

This project was supported by Grant R01 CA111289 from the National Institutes of Health as well as Iowa State University.

Bigelow, T. A. (**2008**). "Ultrasound attenuation estimation using backscattered echoes from multiple sources," J. Acoust. Soc. Am. **124**, 1367–1373.
Bigelow, T. A. (**2010a**). "Improved algorithm for estimation of attenuation along propagation path using backscattered echoes from multiple sources," Ultrasonics **50**, 496–501.
Bigelow, T. A. (**2010b**). "Estimating the total ultrasound attenuation along the propagation path by applying multiple filters to backscattered echoes from a single spherically focused source," IEEE Trans. Ultrason. Ferroelectr. Freq. Control **57**, 900–907.
Bigelow, T. A., McFarlin, B. L., O'Brien, W. D., Jr., and Oelze, M. L. (**2008**). "In vivo ultrasonic attenuation slope estimates for detecting cervical ripening in rats: Preliminary results," J. Acoust. Soc. Am. **123**, 1794–1800.
Bigelow, T. A., and O'Brien, W. D., Jr. (**2004**). "Scatterer size estimation in pulse-echo ultrasound using focused sources: Calibration measurements and phantom experiments," J. Acoust. Soc. Am. **116**, 594–602.
Bigelow, T. A., and O'Brien, W. D., Jr. (**2006**). "Impact of local attenuation approximations when estimating correlation length from backscattered ultrasound echoes," J. Acoust. Soc. Am. **120**, 546–553.
Bigelow, T. A., Oelze, M. L., and O'Brien, W. D., Jr. (**2005**). "Estimation of total attenuation and scatterer size from backscattered ultrasound waveforms," J. Acoust. Soc. Am. **117**, 1431–1439.
Callé, S., Remenieras, J.-P., Matar, O. B., Hachemi, M. E., and Patat, F. (**2005**). "Temporal analysis of tissue displacement induced by a transient ultrasound radiation force," J. Acoust. Soc. Am. **118**, 2829–2840.
Hall, T. J., Insana, M. F., Harrison, L. A., and Cox, G. G. (**1996**). "Ultrasonic measurement of glomerular diameters in normal adult humans," Ultrasound Med. Biol. **22**, 987–997.
He, P. J. F. G. (**1986**). "Application of stochastic analysis to ultrasonic echoes—Estimation of attenuation and tissue heterogeneity from peaks of echo envelope," J. Acoust. Soc. Am. **79**, 526–534.
Insana, M. F., and Hall, T. J. (**1990**). "Parametric ultrasound imaging from backscatter coefficient measurements: Image formation and interpretation," Ultrason. Imaging **12**, 245–267.
Insana, M. F., Wagner, R. F., Brown, D. G., and Hall, T. J. (**1990**). "Describing small-scale structure in random media using pulse-echo ultrasound," J. Acoust. Soc. Am. **87**, 179–192.
Insana, M. F., Zagzebski, J. A., Madsen, E. L., and Frank, G. R. (**1983**). "Analysis of a spectral difference method for measuring the slope of attenuation coefficients," Ultrason. Imaging **5**, 173.
Kuc, R. (**1980**). "Clinical application of an ultrasound attenuation coefficient estimation technique for liver pathology characterization," IEEE Trans. Biomed. Eng. **BME-27**, 312–319.
Lizzi, F. L., Greenebaum, M., Feleppa, E. J., Elbaum, M., and Coleman, D. J. (**1983**). "Theoretical framework for spectrum analysis in ultrasonic tissue characterization," J. Acoust. Soc. Am. **73**, 1366–1373.
Oelze, M. L., O'Brien, W. D., Jr., Blue, J. P., and Zachary, J. F. (**2004**). "Differentiation and characterization of rat mammary fibroadenomas and 4T1 mouse carcinomas using quantitative ultrasound imaging," IEEE Trans. Med. Imaging **23**, 764–771.
Parmar, N, and Kolios, M. C. (**2004**). "Attenuation mapping for monitoring thermal therapy using ultrasound transmission imaging," in Engineering in Medicine and Biology Society, IEMBS '04. 26th Annual International Conference of the IEEE, pp. 1329–1332.
Parmar, N, and Kolios, M. (**2006**). "An investigation of the use of transmission ultrasound to measure acoustic attenuation changes in thermal therapy," Med. Biol. Eng. Comput. **44**, 583–591.
Sidney, D. A. (**1997**). "Three-dimensional ultrasound power deposition modeling, thermal field visualization, and clinical integration of hyperthermia therapy," Ph.D. thesis, Massachusetts Institute of Technology, Cambridge, MA.
Starritt, H. C., Duck, F. A., and Humphrey, V. F. (**1991**). "Forces acting in the direction of propagation in pulsed ultrasound fields," Phys. Med. Biol. **36**, 1465–1474.
Treece, G., Prager, R., and Gee, A. (**2005**). "Ultrasound attenuation measurement in the presence of scatterer variation for reduction of shadowing and enhancement," IEEE Trans. Ultrason. Ferroelectr. Freq. Control **52**, 2346–2360.
Tu, H., Zagzebski, J., and Chen, Q. (**2006**). "Attenuation estimations using envelope echo data: Analysis and simulations," Ultrasound Med. Biol. **32**, 377–386.
Wear, K. A. (**2002**). "A Gaussian framework for modeling effects of frequency-dependent attenuation, frequency-dependent scattering, and gating," IEEE Trans. Ultrason. Ferroelectr. Freq. Control **49**, 1572–1582.
Yao, L. X., Zagzebski, J. A., and Madsen, E. L. (**1990**). "Backscatter coefficient measurements using a reference phantom to extract depth-dependent instrumentation factors," Ultrason. Imaging **12**, 58–70.